A Hybrid Approach Based on Improved AR Model and MAA for INS/DVL Integrated Navigation Systems

DI WANG, XIAOSU XU, YIQING YAO, YONGYUN ZHU, AND JINWU TONG

Key Laboratory of Micro-Inertial Instrument and Advanced Navigation Technology, Ministry of Education, Southeast University, Nanjing 210096, China
School of Instrument Science and Engineering, Southeast University, Nanjing 210096, China

Corresponding author: Xiaosu Xu (xxs@seu.edu.cn)

ABSTRACT In navigation of autonomous underwater vehicles (AUVs), the estimation of position is an important issue, especially, when the sensors such as gyroscopes contain a lot of noise, and the velocity information of Doppler velocity log (DVL) is affected by the motion attitude of the vehicle. In this paper, based on an improved auto regressive (AR) model, a real-time filter is utilized for gyroscope signal denoising. Meanwhile, according to the characteristics of the AUV, the influence of the vehicle attitude on the DVL velocity measurement error is analyzed and a motion attitude assist (MAA) method based on error model is introduced for enhancing DVL velocity accuracy. In this paper, using the proposed hybrid approach, an inertial navigation system (INS)/DVL integrated navigation system is designed. The proposed approach is evaluated by simulation and experimental test in different acceleration bound, and the existence of the DVL outage for an AUV. The results indicate that the precisions of the velocity and position are improved effectively, especially in complex motion attitude and long sailing conditions.

INDEX TERMS Autonomous underwater vehicle (AUV), auto regressive (AR) model, motion attitude assist (MAA), INS/DVL integrated navigation.

I. INTRODUCTION

In recent years, autonomous underwater vehicles (AUVs) have played an important role in military missions such as the ocean exploration. As one of the key technologies for AUV to explore the ocean, navigation is the premise and foundation of all underwater works, which deeply affects the effectiveness and quality of underwater mission execution [1]. With the development of economy, society and military, AUV is getting more and more attention in the direction of long range, high speed, large depth and intelligence. On the one hand, in order to adapt to the corresponding combat missions, the navigation system of AUV must have navigation capabilities of high-precision and long-range. Meanwhile, there are also high requirements in terms of size, power consumption and working time. On the other hand, the precise control of AUV heavily relies on the performance of the

navigation system. Therefore, high-precision attitude, speed and position information must be provided by the AUV navigation system to meet the requirements of underwater operations. In addition, since the AUV cannot obtain satellite navigation signals under water, its navigation performance is further limited compared to the surface vehicle [2]. At present, navigation and positioning technology have become the key to the widespread application of AUV.

Inertial Navigation System (INS) has become the main way to realize the navigation of autonomous underwater vehicles by its autonomy and concealment characteristics [3]. INS is an autonomous system, which includes three accelerometers and three gyroscopes measuring respectively the linear acceleration and angular rate of the motion of vehicles. The navigation frame is established according to the output of the gyroscopes. Meanwhile, the velocity and position of the vehicle are calculated according to the output of the accelerometers. The inertial navigation system can provide all-round navigation information such as attitude, speed and

---

The associate editor coordinating the review of this manuscript and approving it for publication was Bora Onat.

position, which has the advantage that other navigation methods do not have. In the navigation system of AUV, the INS has always been the preferred method adopted by various countries, which is the leading navigation system in a variety of navigation fusion systems.

The existing underwater navigation methods are mainly divided into three categories: dead reckoning and inertial navigation, acoustic navigation and geophysical navigation [4]. These different navigation methods can be used individually or in combination to improve navigation accuracy. In underwater integrated navigation, other sensors, such as Long Baseline (LBL), Ultra Short Baseline (USBL), Doppler Velocity Log (DVL), and Global Navigation Satellite System (GNSS), are usually assisted on the basis of INS. Meanwhile, LBL, in which a vehicle triangulates its position from acoustic ranges within a network of surveyed transponders, and USBL, in which a sonar array is employed to determine the range and bearing to the vehicle, both need priori deployments [5]. However, it is impossible to pre-deploy transponders in most unknown underwater environments. Therefore, based on the INS and assisted by the DVL equipment, it becomes a common method for the AUV navigation system. This technology has been rapidly developed in recent years since it was successfully applied at the MARIDAN AUV in Denmark at the beginning of this century.

In terms of the INS/DVL integrated navigation fusion algorithm, Reference [6] presents an approach for aiding the INS of an underwater vehicle using velocity measurements provided by an experimentally validated kinetic vehicle model. It is claimed in [7] that the localization of an AUV is performed using two different forms of Kalman filter (KF): extended Kalman filter (EKF) and unscented Kalman filter (UKF), meanwhile, their estimates are compared. In addition, a method based on INS/DVL is proposed. A 15-state INS error model and corresponding measurement model of aiding devices are derived for the KF, which can be seen in the existing Reference [8]. Reference [9] focuses on the problem of predicting the observable and unobservable error states of AUV navigation system for several maneuvering types, particularly for an INS assisted by a DVL and a pressure sensor (PS). An asynchronous adaptive direct Kalman filter algorithm is introduced in [10] to improve underwater navigation system performance. According to Reference [11], a simplified algorithm is proposed for reducing the computational load of the conventional underwater integrated navigation system, which based on a three-dimensional accelerometer, a three-dimensional gyroscope, and a three-dimensional Doppler velocity log. Liu *et al.* [12] employ a Kalman filter for cross-noise and the forming mechanism of cross-noise in INS/DVL is studied in detail. The proposed algorithm in [13] is based on zero velocity update (ZUPT) and interactive multiple model (IMM) while DVL outage. In Reference [14] a Square-Root unscented information filter is suggested and applied in SINS/DVL Integrated Navigation.

In terms of fault tolerance algorithm for the INS/DVL integrated navigation, Reference [15] proposes a DVL-based vehicle velocity solution using the measured partial raw data of the DVL and additional information, thereby deriving an extended loosely coupled approach. Liu *et al.* [16] suggest a fast gradual fault detection method based on the improved residual χ^2 detection algorithm for underwater integrated navigation systems. In Reference [17] a fault-tolerant adaptive Kalman filter (FTAKF) algorithm is designed for INS composed of an INS, a DVL, and a magnetic compass (MCP). The evolutionary artificial neural networks (EANN) is used in self-learning and training of the intelligent data fusion algorithm. According to Reference [18], an adaptive robust Kalman filter (ARKF) based on hybrid-correction grid INS/DVL integrated navigation algorithm is proposed with the unified reference ellipsoid Earth model to improve the navigation accuracy in middle-high latitude regions for marine applications. A hybrid approach is presented to forecast the measurements of the DVL while it malfunctions in [19], which employs partial least squares regression (PLSR) coupled with support vector regression (SVR) to build a hybrid predictor. An INS/DVL/PS tightly coupled underwater navigation method with Limited DVL Measurements is introduced in [20].

Although the above research have improved the accuracy of INS/DVL integrated navigation, the following problems are still exist:

1. Most of the algorithms are based on the data acquired by the gyroscope, but not considering that noises of the gyroscope are the main reasons for accumulations of errors in the INS.

2. In the integrated system, the velocity of DVL is projected from the vehicle frame to the navigation frame by only using the course information (such as roll and pitch) provided by INS or attitude reference system and ignoring the vehicle's attitude dynamics.

In response to the above problems, a hybrid approach is proposed based on an improved auto regressive (AR) model and motion attitude assist (MAA) for INS/DVL integrated navigation system. On the one hand, an AR online modeling method based on gyro signals is designed, and the improved recursive least squares algorithm is introduced to realize parameter identification. This method can effectively de-nosing gyro signals and reduce random drift error. On the other hand, the influence mechanism of the AUV motion attitude on the DVL velocity measurement is analyzed. In addition, a DVL velocity measurement method based on motion attitude assist is proposed.

The rest of this paper are organized as follows: The INS/DVL integrated navigation system and the proposed hybrid approach are described in Section 2. Section 3 introduces the improved AR model for gyro random drift error. Motion attitude assisted DVL solution is introduced in Section 4. In Section 5, the results are given for simulation and vehicle tests to verify the proposed hybrid approach. Finally, conclusions are drawn in section 6.

II. INS/DVL INTEGRATED NAVIGATION SYSTEM

A. SYSTEM STRUCTURE AND MODEL

The INS has the complete autonomous navigation capabilities to meet the hidden requirements of underwater vehicles. However, the pure use of INS has inherent drawbacks that navigation errors accumulate over time. Therefore, the integrated navigation system based on INS has become a development trend. The high-precision velocity information is provided by DVL to suppress the accumulation of INS errors in INS/DVL integrated navigation systems. It has the characteristics of good autonomy and high positioning accuracy.

In the INS/DVL integrated navigation system, the velocity obtained by the INS solution is in the navigation frame. However the velocity measured by the DVL is in the body frame. Therefore, after the attitude transition matrix C_b^n solved by the INS is used to convert the measured velocity of the DVL to the navigation frame. The differences between the velocity of the INS solution and the velocity of the DVL in the navigation frame are used as the observation of the Kalman filter. Finally, the Kalman filter is used to estimate the error state quantities such as attitude, velocity and position for closed-loop correction. The schematic diagram of the INS/DVL integrated navigation system is shown in Figure 1.
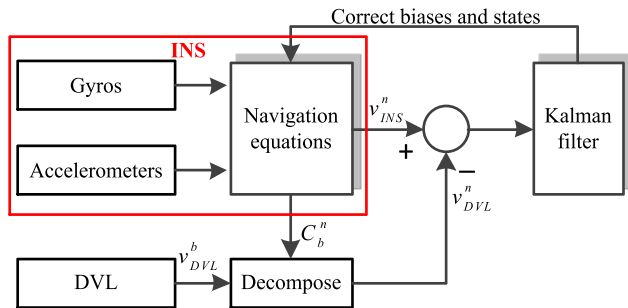

FIGURE 1. INS/DVL integrated navigation system.

Taking the Right-Front-Up (RFU) frame as body frame, and the East-North-Up (ENU) geographic coordinates as navigation frame. The error state vector of the INS/DVL integrated navigation system can be set as [12]:

$$X_k = [\phi_E \ \phi_N \ \phi_U \ \delta v_E \ \delta v_N \ \delta v_U \ \delta L \ \delta \lambda \ \delta h$$
$$\varepsilon_x \ \varepsilon_y \ \varepsilon_z \ \nabla_x \ \nabla_y \ \nabla_z] \quad (1)$$

where ϕ_E, ϕ_N, ϕ_U represent misalignment angles of the calculated platform in n frame, $\delta v_E, \delta v_N, \delta v_U$ represent velocity errors, $\delta L, \delta \lambda, \delta h$ represent the latitude, longitude and height errors, respectively, $\varepsilon_x, \varepsilon_y, \varepsilon_z$ represent gyroscope biases in three directions of the frame b, $\nabla_x, \nabla_y, \nabla_z$ represent accelerometer biases in b frame.

The system model for the Kalman filter can be described as follows:

$$\begin{cases} X_k = \Phi_{k,k-1} X_{k-1} + W_k \\ Z_k = H_k X_k + V_k \end{cases} \quad (2)$$

where X_{k-1} is the state vector of the integrated navigation system at time t_{k-1}, and X_k is the state vector at time t_k, Z_k is the measurement vector, $\Phi_{k,k-1}$ is the system dynamic model from time t_{k-1} to t_k, H_k is the measurement transfer matrix, $W_k \sim N(0, Q_k)$ is the process noise, and $V_k \sim N(0, R_k)$ is the measurement noise, Q_k and R_k are the variance matrix of the process noise and the measurement noise respectively. For the sake of research, the noise caused by the underwater environment is assumed to be white noise.

The integration of the DVL and the INS is processed in the Kalman filter, and the measurement vector can be constructed as:

$$Z_k = \begin{bmatrix} v_{INSE}^n - v_{DVLE}^n & v_{INSN}^n - v_{DVLN}^n & v_{INSU}^n - v_{DVLU}^n \end{bmatrix}^T \quad (3)$$

where the superscript n denotes the navigation frame. As mentioned, the DVL provides the velocity measurements in the body frame and hence the measurement values could not be used as the measurement for alignment directly, $v_{DVL}^n = [v_{DVLE}^n \ v_{DVLN}^n \ v_{DVLU}^n]$ is the projected velocity of the DVL measurements in the navigation frame, which can be calculated as follows:

$$\begin{cases} v_{DVL}^n = C_b^n v_{DVL}^b \\ C_b^n = \tilde{C}_b^n \cdot [\phi \times] \end{cases} \quad (4)$$

where the DVL velocity measurements in the body frame is v_{DVL}^b, C_b^n is the direction cosine matrix of transformation from the body frame b to the navigation frame n, from which the attitude of the vehicle can be extracted. $\tilde{C}_b^n$ represent direction cosine matrix calculated by measurement information. ϕ represent attitude error angles. According to the relationship between the measurement vector and the error state vector, the measurement matrix of the Kalman filter can be derived as follows:

$$H_k = \begin{bmatrix} 0_{3 \times 3} & I_{3 \times 3} & 0_{3 \times 9} \end{bmatrix} \quad (5)$$

where $I_{3 \times 3}$ is an 3×3 identity matrix, $0_{m \times n}$ is a zero matrix with m rows and n columns.

B. PROPOSED HYBRID APPROACH

Some DVLs can measure roll and pitch angles and correct the resulting error. However, the attitude accuracy is not better than the attitude provide by INS. And there is no public information showing which method is used for compensation. According to the above analysis, the accuracy of INS/DVL integrated navigation is affected by two aspects without considering the data fusion algorithm: the noise of the gyroscope and accelerometer, and the DVL velocity error. Since the velocity obtained by the DVL measurement is in the body frame, and the direction cosine matrix C_b^n needs to be passed to obtain the final velocity in the navigation frame. Therefore, the velocity accuracy of DVL is affected by its own measurement accuracy and direction cosine matrix C_b^n, and C_b^n is obtained by INS calculation through gyro signal. In summary, the accuracy of the gyro signal in the INS/DVL integrated navigation system affects the accuracy of the INS and DVL outputs. At the same time, the velocity error of DVL

in the body frame also has a great influence on the accuracy of the integrated navigation system. Therefore, to improve the accuracy of integrated navigation two aspects are introduced in this paper. First, the gyro is de-noised to improve the performance of the gyro signal. Second, a DVL error compensation model is established to improve the accuracy of the velocity. The entire system block diagram is shown in Figure 2.
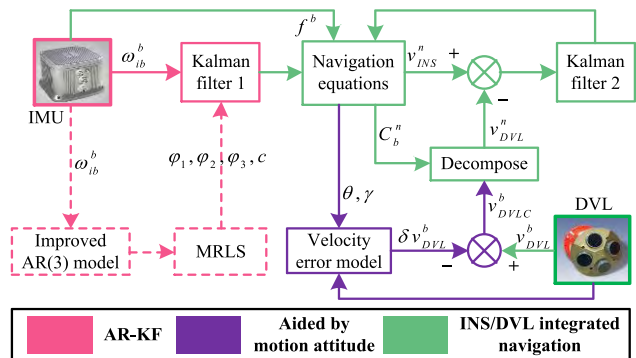

FIGURE 2. Diagram of the proposed hybrid approach.

It can be seen from Figure 2 that the hybrid approach proposed in this paper is divided into three parts: the gyro de-noising part drawn by the red line, the DVL speed measurement error compensation part of the motion attitude assisted by the purple line as well as the INS/DVL integrated navigation drawn by the cyan line. The detail steps are as follows:

1. The gyro signal real time de-noising method. Firstly, an improved AR (3) model is built. Then, after power-on, the gyro output data is collected for a period of time as the signal input of the AR model and the parameter recognition of the AR model is realized by the modified RLS algorithm. Finally, the identification parameters are introduced into the Kalman filter 1. At this time, the Kalman filter 1 can perform filtering processing on the three-axis gyro signals in real time.

2. DVL speed measurement error compensation method by motion attitude assisted. The DVL velocity measurement error model is established, basing on the motion attitude. The DVL velocity error is compensated by the attitude information obtaining from the INS solution, and then the compensated DVL velocity is converted to the navigation frame by the attitude transition matrix.

3. INS/DVL integrated navigation information fusion processing. According to the above two steps, the velocity under the navigation frame obtained by the INS and DVL are used as the measurement inputs of the Kalman filter 2. Meanwhile, the estimated results of Kalman filter 2 are feedback into the INS solution to correct the error.

III. IMPROVED AR MODEL FOR GYRO RANDOM DRIFT ERROR
A. ONLINE MODELING BASED AR MODEL
The framework of the AR (n) model is [21]:

$$x_k = \varphi_1 x_{k-1} + \varphi_2 x_{k-2} + \cdots + \varphi_n x_{k-n} + a_k \quad (6)$$

where $\varphi_1 \sim \varphi_n$ represent parameters to be estimated, k represents the sequence number, a_k represents white noise. On the assumption that the collected fiber optic gyroscope (FOG) signals $z_1, z_2 \cdots z_k, z_{k+1} \cdots$ are stationary and a normal sequence, the AR model can be established by the traditional method with a zero mean value. The observed time series can be written after subtracting the mean value as follows:

$$x_{k-n} = z_{k-n} - \bar{z} \quad (n = 0, 1, 2, \cdots) \quad (7)$$

where $\bar{z}$ represents the mean value. By bringing the formula (7) into the formula (6), the following formula is obtained:

$$z_k = \varphi_1 z_{k-1} + \varphi_2 z_{k-2} + \cdots + \varphi_n z_{k-n}$$
$$+ (1 - \varphi_1 - \varphi_2 - \cdots - \varphi_n) \cdot \bar{z} + a_k \quad (8)$$

From the above theoretical analysis, we can know that the average value $\bar{z}$ of the FOG static output data should be constant after gyroscope stabilization after restarting. After the model is established, $\varphi_1 \sim \varphi_n$ are also constant, so we denote:

$$c = (1 - \varphi_1 - \varphi_2 - \cdots - \varphi_n) \cdot \bar{z} \quad (9)$$

By writing Equation (9) into Equation (8), then, the Equation (8) can be rewritten as:

$$z_k = \varphi_1 z_{k-1} + \varphi_2 z_{k-2} + \cdots + \varphi_n z_{k-n} + c + a_k \quad (10)$$

The above Formula is a dynamic AR model. The recursive least squares (RLS) algorithm and the modified recursive least squares (MRLS) algorithm are introduced to estimate unknown parameters $\varphi_1, \varphi_2, \cdots \varphi_n, c$ in real time.

B. MODIFIED RLS FOR MODEL PARAMETERS ESTIMATION
The AR model parameter estimation methods fall into two categories: the first type of method is the direct estimation method, which directly estimates the model parameters based on the observed data, and the most common method is the least squares (LS) method. This method relies on experience to select data. The sampling time is less accurate than the model parameter estimation. The long sampling time cannot meet the real-time requirements. The second type of method is the recursive estimation method, which can estimate the model parameters in real time. This section firstly introduces the RLS method to estimate the parameters of the FOG gyro random drift model.

Substituting the collected FOG output $\{z_k, k = 1, 2, \cdots, N\}$ at the initial time into equation (10), then the linear equations can be written as follows [22]:

$$\begin{cases} z_{n+1} = \varphi_1 z_n + \varphi_2 z_{n-1} + \cdots + \varphi_n z_1 + c + a_{n+1} \\ z_{n+2} = \varphi_1 z_{n+1} + \varphi_2 z_n + \cdots + \varphi_n z_2 + c + a_{n+2} \\ \cdots \\ z_N = \varphi_1 z_{N-1} + \varphi_2 z_{N-n} + \cdots + \varphi_n z_{N-n} + c + a_N \end{cases} \quad (11)$$

The Equation (11) is expressed in matrix form as:

$$\boldsymbol{Y}_N = \boldsymbol{Z}_N \boldsymbol{\theta}_N + \boldsymbol{a}_N \quad (12)$$

where,

$$\begin{cases} \boldsymbol{Y}_N = \begin{bmatrix} z_{n+1} \ z_{n+2} \ \cdots \ z_N \end{bmatrix}^T_{1\times(N-n)'} \\ \boldsymbol{\theta}_N = \begin{bmatrix} \varphi_1 \ \varphi_2 \ \cdots \ \varphi_n \ c \end{bmatrix}^T_{1\times(n+1)'} \\ \boldsymbol{a}_N = \begin{bmatrix} a_{n+1} \ a_{n+2} \ \cdots \ a_N \end{bmatrix}^T_{1\times(N-n)'}, \\ \boldsymbol{Z}_N = \begin{bmatrix} z_n & z_{n-1} & \cdots & z_1 & 1 \\ z_{n+1} & z_n & \cdots & z_2 & 1 \\ \cdots & & & & \\ z_{N-1} & z_{N-2} & \cdots & z_{N-n} & 1 \end{bmatrix} \end{cases} \quad (13)$$

According to the theory of multiple regression, the LS estimation of the parameter matrix $\boldsymbol{\theta}_N$ can be expressed as:

$$\boldsymbol{\theta}_N = \left(\boldsymbol{Z}_N^T \boldsymbol{Z}_N \right)^{-1} \boldsymbol{Z}_N^T \boldsymbol{Y}_N \quad (14)$$

Assuming that $\boldsymbol{\theta}_N$ is the model parameter of the observed sequence at the present stage and with the arrival of new data z_{N+1}, an updated estimation of $\boldsymbol{\theta}_N$ can be obtained based on sequence $\{z_t, t = 1, 2, \cdots, N, N + 1\}$. According to the form of the above matrix, the LS estimation based on $N + 1$ data is as follows [21]:

$$\begin{cases} \boldsymbol{\theta}_{N+1} = \boldsymbol{p}_{N+1} \boldsymbol{Z}_{N+1}^T \boldsymbol{Y}_{N+1} \\ \boldsymbol{p}_{N+1} = \left(\boldsymbol{Z}_{N+1}^T \boldsymbol{Z}_{N+1} \right)^{-1} \end{cases} \quad (15)$$

where,

$$\begin{cases} \boldsymbol{Z}_{N+1} = \begin{bmatrix} \boldsymbol{Z}_N \\ \boldsymbol{Z}_{(h+1)} \end{bmatrix}'_{(N-n+1)\times(n+1)}, \\ \boldsymbol{Y}_{N+1} = \begin{bmatrix} \boldsymbol{Y}_N \\ z_{N+1} \end{bmatrix}_{(N-n+1)\times 1} \\ \boldsymbol{Z}_{(h+1)} = \begin{bmatrix} z_N \ z_{N-1} \ \cdots \ z_{N-n+1} \ 1 \end{bmatrix}_{1\times(n+1)} \end{cases} \quad (16)$$

where h is sequence number, and its range is $[1, +\infty]$. According to the multiplication of the block matrix, the following expression can be described as:

$$\begin{cases} \boldsymbol{Z}_{N+1}^T \boldsymbol{Y}_{N+1} = \boldsymbol{Z}_N^T \boldsymbol{Y}_N + \boldsymbol{Z}_{(h+1)}^T z_{N+1} \\ \boldsymbol{p}_{N+1} = (\boldsymbol{p}_N^{-1} + \boldsymbol{Z}_{(h+1)}^T \boldsymbol{Z}_{(h+1)})^{-1} \end{cases} \quad (17)$$

The following expression can be obtained by the matrix inversion formula:

$$\boldsymbol{p}_{N+1} = \left(\boldsymbol{I} + \boldsymbol{p}_N \frac{\boldsymbol{Z}_{(h+1)}^T \boldsymbol{Z}_{(h+1)}}{1 + \boldsymbol{Z}_{(h+1)} \boldsymbol{p}_N \boldsymbol{Z}_{(h+1)}^T} \right) \boldsymbol{p}_N \quad (18)$$

where $\boldsymbol{I}_{(n+1)\times(n+1)}$ represents an identity matrix.

Substituting Equations (17) and (18) into Equation (15), the recursive estimation formula of the parameters can be described as:

$$\boldsymbol{\theta}_{N+1} = \boldsymbol{\theta}_N + \boldsymbol{K}_{N+1} \left(z_{N+1} - \boldsymbol{Z}_{(h+1)} \boldsymbol{\theta}_N \right) \quad (19)$$

where,

$$\boldsymbol{K}_{N+1} = \frac{1}{1 + \boldsymbol{Z}_{(h+1)} \boldsymbol{p}_N \boldsymbol{Z}_{(h+1)}^T} \boldsymbol{p}_N \boldsymbol{Z}_{(h+1)}^T \quad (20)$$

The formula (19) shows that the new estimation $\boldsymbol{\theta}_{N+1}$ of the AR model parameters involves amending the original estimation $\boldsymbol{\theta}_N$, and the correction term is $\boldsymbol{K}_{N+1} \left(z_{N+1} - \boldsymbol{Z}_{(h+1)} \boldsymbol{\theta}_N \right)$.

This paper proposes a modified recursive least squares (MRLS) algorithm by introducing the fading factor λ. Because the fading factor λ plays an important role in the performance of the entire system, it is possible to consider modifying λ so that it can both enhance the tracking ability of the system and make the estimation error of the system convergence small. Therefore, the idea of using a fading factor is considered. The Equation (18) can be described as:

$$\boldsymbol{p}_{N+1} = \lambda \left(\boldsymbol{I} + \boldsymbol{p}_N \frac{\boldsymbol{Z}_{(h+1)}^T \boldsymbol{Z}_{(h+1)}}{1 + \boldsymbol{Z}_{(h+1)} \boldsymbol{p}_N \boldsymbol{Z}_{(h+1)}^T} \right) \boldsymbol{p}_N \quad (21)$$

When the error becomes small, λ is close to 1, which will reduce the error of the parameter. Otherwise, when the error becomes larger, λ becomes smaller. We set its minimum value to $\lambda_{\min}$, which will strengthen the tracking ability of the system. Based on the understanding of λ, this paper proposes the following ideas: since the magnitude of the λ value can be determined by the error, an error point can be found, such as the error mean $E[e(n)]$. When it is less than this value, λ is closer to 1 by a curve. When it is greater than this value, λ is approximated by $\lambda_{\min}$ and a curve, as shown in Figure 3. We call it a correction function, which can be represented by an inverse cotangent function. The function expression is as follows:

$$e(n) = z_{N+1} - \boldsymbol{Z}_{(h+1)} \boldsymbol{\theta}_N \quad (22)$$

$$\lambda = \frac{1 - \lambda_{\min}}{\pi} \text{arc cot} \{e(n) - E[e(n)]\} + \lambda_{\min} \quad (23)$$
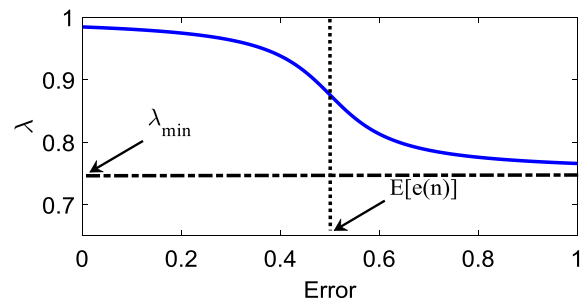
FIGURE 3. Curve of correct function.

It can be seen from the correction function that the fading factor λ is controlled by the error, which can ensure that the error swings around $E[e(n)]$, and the change is slow, which can buffer the poor tracking effect caused by the λ change too fast. The problem, so after the iteration, plus the correction of this correction function, the advantages of the variable forgetting factor RLS algorithm can be maintained.

C. REAL TIME DE-NOISING ALGORITHM BASED ON IMPROVED AR MODEL

The noise brought by the gyro can be divided into two types from the frequency domain analysis: long-term noise

and short-term noise. In the INS/DVL integrated navigation system, the Kalman filter can estimate the gyro constant drift error, thus eliminating some of the long-term noise. On the one hand, as unmanned submersibles navigate in complex, unknown underwater conditions, short-term noise can be present in the presence of surrounding obstacles, water currents, and the like. On the other hand, the INS solution can be considered as an integration process and therefore has the function of a low-pass filter. At this time, the short-term noise in the INS/DVL integrated navigation system is filtered by the low-pass filter during the INS navigation solution. The entire schematic is shown in Figure 4.
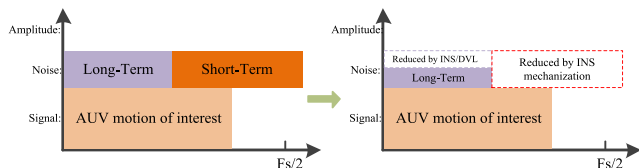
FIGURE 4. Schematic plot of inertial signal in frequency domain.

As can be seen from the Figure 4, some of the long-term noise (low-frequency noise) is not eliminated, which contains constant drift noise, random drift noise and a small amount of colored noise. Constant drift noise can be handled by calibration compensation or carried out by the manufacturers. So, the random drift noise is main error source for INS. Most of the research makes a first-order Markov process for the low-frequency correlated noise of the gyroscope, but in fact the first-order Markov process cannot fully reflect the random drift of the inertial device. Therefore, the low frequency residual noise of the gyroscope can be further eliminated by the AR model.

The results show that the AR (3) model can fit the FOG random drift well in [23], so the improved AR (3) model is used to model online. Kalman filtering is performed directly on the FOG signal. The improved AR(3) model has a constant c due to the replacement of the zero-mean signal with the FOG measured signal. This paper also considers c as a state variable. Therefore, the system state equation can be expressed as:

$$X_k = A X_{k-1} + B W_k \qquad (24)$$

where $X_k = \begin{bmatrix} z_k & z_{k-1} & z_{k-2} & c \end{bmatrix}^T_{1 \times 4}$ presents state vector, $W_k = \begin{bmatrix} a_k & 0 & 0 & 0 \end{bmatrix}^T_{1 \times 4}$ presents process noise [24].

$$A = \begin{bmatrix} \varphi_1 & \varphi_2 & \varphi_3 & 1 \\ 1 & 0 & 0 & 0 \\ 0 & 1 & 0 & 0 \\ 0 & 0 & 0 & 1 \end{bmatrix}_{4 \times 4}, B = \begin{bmatrix} 1 & 0 & 0 & 0 \\ 0 & 0 & 0 & 0 \\ 0 & 0 & 0 & 0 \\ 0 & 0 & 0 & 0 \end{bmatrix}_{4 \times 4} \qquad (25)$$

Supposing that the FOG signal is Z_k, then the measurement equation of the system can be described as:

$$Z_k = H X_k + V_k \qquad (26)$$

where $H = \begin{bmatrix} 1 & 0 & 0 & 0 \end{bmatrix}_{1 \times 4}$, and V_k is measurement noise.

IV. MOTION ATTITUDE ASSISTED DVL SOLUTION
A. THE PRINCIPLE OF DVL MEASUREMENT
The DVL emits ultrasonic waves to the sea floor by an acoustic sensor mounted on the vehicle, and measures the body velocity based on the Doppler Effect principle.

Assuming that frequency of transmitting acoustic signals of DVL is f_0 and wave speed is c_0. The horizontal velocity of vehicle is v_x, which is described in Figure 5. Defining Doppler shift is [21], [24]:

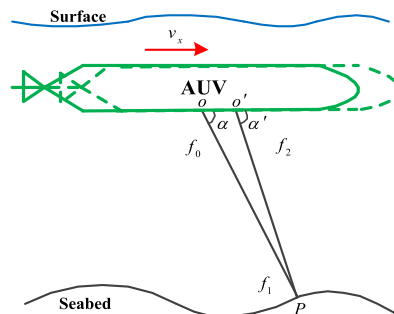$$v_x = \frac{c_0 f_d}{2 f_0 \cos \alpha} \qquad (27)$$

FIGURE 5. The principle of DVL measurement.

B. ERROR MODEL AIDED BY MOTION ATTITUDE
The vehicle motion attitude error is that Doppler acoustic wave launch angle will change and cause velocity calculation error when the vehicle is shaken by the action of external water waves during operation. In the dual-beam configuration, taking beam #1 and beam #3 as an example, the velocity measurement error caused by the vehicle's pitch change along the vehicle axis is analyzed. The beam tilt angle denotes that the angle between the acoustic beam emitted by the Doppler and the horizontal plane. Figure 6 shows a schematic diagram of the change in the beam tilt caused by the vehicle's swing.
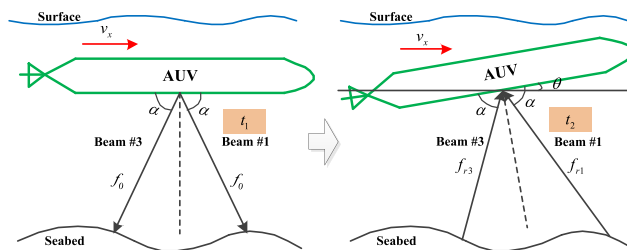

FIGURE 6. The change in beam tilt caused by the pitch angle.

In the process of analysis and modeling, the changes of angular between the signal transmission and reception instant are considered in this section. According to the principle of DVL, the pitch angle in each of the two beam (#1 and #3) directions at transmission instant t_1 and reception instant t_2 can be respectively expressed as θ and $-\theta$. As shown

in Figure 6, the slope of beam #1 is calculated using an inclination angle of α and the actual beam slope is $(\alpha - \theta)$. Similarly, the actual beam tilt angle of beam #3 is $(\alpha + \theta)$. According to formula (27), the Doppler shift may be found as:

$$f_d = \frac{2v_x \left(\cos\left(\alpha - \theta\right) + \cos\left(\alpha + \theta\right)\right)}{c_0} f_0 \qquad (28)$$

The velocity of vehicle forward is:

$$v_x = \frac{c_0 f_d}{2 f_0 \left(\cos\left(\alpha - \theta\right) + \cos\left(\alpha + \theta\right)\right)} = \frac{c_0 f_d}{4 f_0 \cos\alpha \cos\theta} \qquad (29)$$

Form Equations (28) and (29) the relative velocity error coursed by pitch change for vehicle is:

$$\tau = \frac{\frac{c_0 f_d}{4 f_0 \cos\alpha \cos\theta} - \frac{c_0 f_d}{4 f_0 \cos\alpha}}{\frac{c_0 f_d}{4 f_0 \cos\alpha}} = \frac{1 - \cos\theta}{\cos\theta} \qquad (30)$$
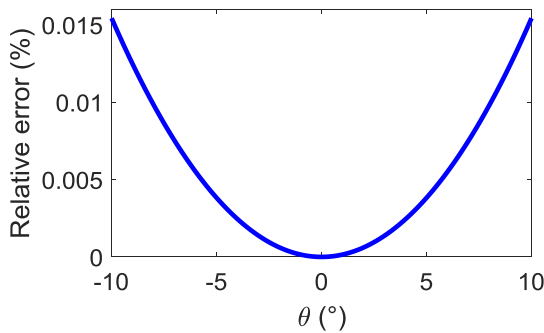
FIGURE 7. The relationship between relative velocity error and pitch angle.

Figure 7 shows the relationship between relative velocity τ and pitch angle θ when θ change from -10° to 10°. As the absolute value of the pitch angle increases, the relative velocity error increases [25]–[27]. When the underwater vehicle swings large caused by sea water fluctuates, the beam tilt angle will constantly change, making the relative speed error larger. This phenomenon is even more pronounced when DVL equipment is used on ship.

Similarly, the relative velocity error will also increase when the roll angle γ changes. At the same time, the influence of the pitch and roll angle on the relative velocity error is considered. The curve is shown in Figure 8.

According to Equation (30), we can get the DVL velocity error compensation formula:

$$\begin{bmatrix} v_{DVLx}^b \\ v_{DVLy}^b \\ v_{DVLz}^b \end{bmatrix} = \begin{bmatrix} 1 & 0 & 0 \\ 0 & 1 - \dfrac{1 - \cos\theta}{\cos\theta} - \dfrac{1 - \cos\gamma}{\cos\gamma} & 0 \\ 0 & 0 & 1 \end{bmatrix} \cdot \begin{bmatrix} v_{DVLx}^b \\ v_{DVLy}^b \\ v_{DVLz}^b \end{bmatrix} \qquad (31)$$

$$\boldsymbol{v}_{DVL}^b = [v_{DVLx}^b \ v_{DVLy}^b \ v_{DVLz}^b]^T \qquad (32)$$

where v_{DVLx}^b, v_{DVLy}^b, v_{DVLz}^b denote the DVL velocity in x, y, and z direction in the body frame.

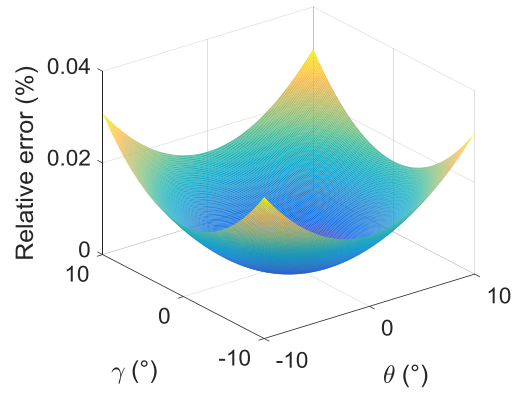According to the above analysis, in the INS/DVL integrated navigation systems, the relative velocity error

FIGURE 8. The relationship between relative velocity error and attitude angle.

Equation (31) can be introduced into the DVL velocity information, thereby improving the speed measurement accuracy of the DVL during the vehicle swing.

V. EXPERIMENTAL RESULTS AND DISCUSSIONS

In order to fully verify the excellent performance of the proposed approach, simulation and vehicle test experiment are designed. In the simulation, firstly, the accuracy and convergence of the parameter identification by RLS algorithm and MRLS algorithm are verified through the simulated time series function. Secondly, the super performance of the MAA method is verified by simulating the vehicle rocking motion in medium sea conditions. In the vehicle test experiment, on the one hand, the effect of the improved AR model is verified for INS/DVL integrated navigation system. On the other hand, the performance of the proposed approach is verified by two scenarios (DVL data normality and DVL outage).

A. SIMULATION
1) MRLS FOR AR MODEL PARAMETERS
First, the time series function obtained by simulation is:

$$z_k = -1.5 z_{k-1} + 0.7 z_{k-2} - 0.2 z_{k-3} + a_k \qquad (33)$$

where z_k is the tested time series, a_k is white noise. From the Equation (33), we can know that the model parameters are $\varphi_1 = -1.5$, $\varphi_2 = 0.7$, $\varphi_3 = -0.2$. The curve of simulation test sequence z_k is shown in Figure 9, where the number of samples are 400.

Second, in order to determine the value of parameter $\lambda_{\min}$ in the proposed MRLS algorithm. Taking the parameter φ_1 in the time series function as the example, two curves are drawn respectively: the relationship between the parameter identification error and the parameter $\lambda_{\min}$, the relationship between the number of sampling points required for convergence and the parameter $\lambda_{\min}$. Figure 10 shows that as the value of $\lambda_{\min}$ increases, the MRLS algorithm accuracy becomes higher and higher, however its convergence speed becomes slower and slower. The intersection of the two curves in the figure (between 0.7 and 0.8) indicates that the accuracy and
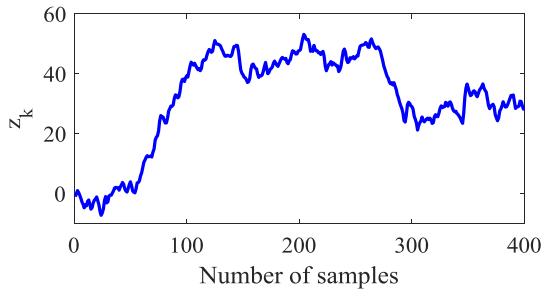
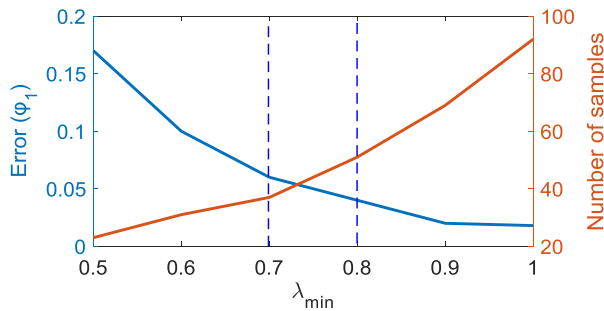**FIGURE 9.** Curve of simulation test sequence.

FIGURE 10. The setting strategy of parameter λ_{min}.

convergence speed of the MRLS algorithm can have a good effect. Therefore, in this paper set $\lambda_{min} = 0.75$. According to above analysis, λ can be adjusted from 1 to 0.75. According to Equation (23), the adjustment strategy of λ can be expressed as: the error mean $E[e(n)]$ is used as the error point. When the result less than this value, λ is closer to 1 according to figure 3. When the result greater than this value, λ is closer to 0.75.
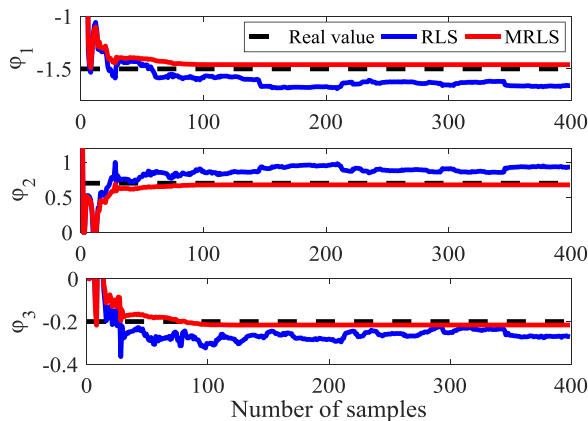
FIGURE 11. Curve of the parameters estimation for different algorithms.

Third, two algorithms (RLS and MRLS) are designed to estimate the model parameters of simulation time series by Equation (42). The results are shown in Figure 11, where the real values, RLS, and MRLS are marked by black lines, blue lines, and red lines respectably. There are three model parameters $\varphi_1, \varphi_2, \varphi_3$. From the Figure we can see that the

TABLE 1. The results of two algorithms.

Parameters	Real value	RLS	MRLS
φ_1	-1.5	-1.65827	-1.45988
φ_2	0.7	0.92966	0.676713
φ_3	-0.2	-0.271283	-0.216165

estimated results are closer to the real value and good stability by MRLS algorithm.

Finally, in order to more clearly compare the performance of the two algorithms. The following Table 1 gives a result of estimating parameters, where we know that the absolute differences between the MRLS results and the real values are: 0.0287, 0.0579, and 0.0496 respectively. However, the calculated results between RLS and the real values are: 0.0576, 0.1285, and 0.0691 respectively. Therefore, the MRLS algorithm has a better accuracy than RLS algorithm for Parameter Estimation.
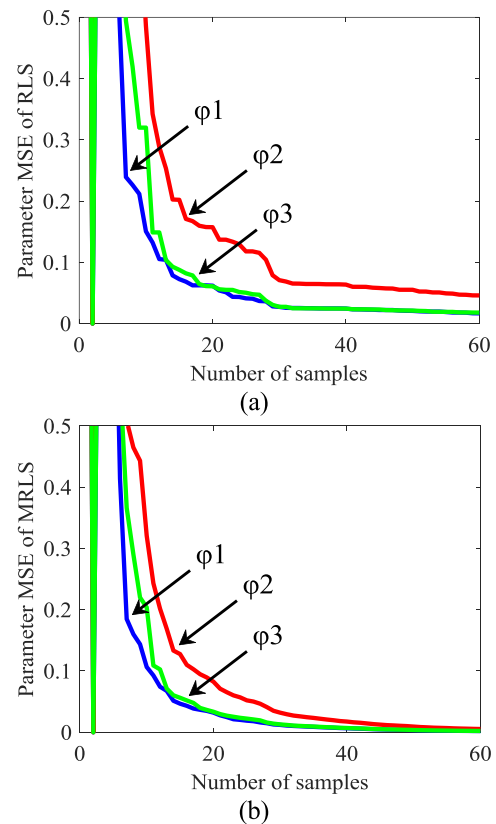

FIGURE 12. Curve of the parameter MSE for different algorithms.

The parameters mean squared error (MSE) are analyzed in Figure 12 to illustrate the convergence. From the figure we know that the parameter MSE of MRLS is better than RLS, and the MRLS has better convergence when the number of samples is 60.

To further illustrate the performance of the MRLS algorithm, a new method is introduced for comparison, which named Yule-Walker and proposed in Reference [28] in 2018.

TABLE 2. The results of three algorithms.

| Method	Number of samples			Error		
	φ_1	φ_2	φ_3	φ_1	φ_2	φ_3
Yule-Walker	175	182	169	0.05	0.12	0.04
RLS	95	110	95	0.15	0.22	0.05
MRLS	42	43	42	0.05	0.03	0.01

Table 2 gives the results of three algorithms, where number of samples denote that the sample size when the parameters are identified. It can be seen that compared with the RLS algorithm, the Yule-Walker requires more samples to successfully identify the parameters, however, the parameters identification accuracy of the Yule-Walker is higher than RLS algorithm. Compared with the MRLS algorithm, the parameters identification accuracy and the number of samples of the proposed MRLS algorithm are better than the Yule-Walker.

2) MAA FOR INS/DVL INTEGRATED NAVIGATION SYSTEM

The whole simulation time lasts for 2000s, which includes acceleration, deceleration, uniform and turning motion. The geographic latitude and longitude of the vehicle are set as 32.05° and 118.79° respectively. The initial velocity is 0m/s. The initial attitudes are $\theta = 0°, \gamma = 0°, \psi = 0°$, and the initial errors of the attitude are $\delta\theta = 0.01°, \delta\gamma = 0.013°, \delta\psi = 0.1°$. The installation errors between IMU and DVL is $\phi_x = 0.002°, \phi_y = 0.003°, \phi_z = 0.08°$. To simulate the medium sea level, the attitude angles of the vehicle are as follow:

$$\begin{cases} \theta = \theta_m \sin\left(\dfrac{2\pi}{5}t + \theta_0\right) \\ \gamma = \gamma_m \sin\left(\dfrac{2\pi}{7}t + \gamma_0\right) \\ \psi = \psi_m \sin\left(\dfrac{2\pi}{6}t + \psi_0\right) \end{cases} \qquad (34)$$

where $\theta_m = 4°, \gamma_m = 5°$, and $\psi_m = 3°$ are the amplitude of the swaying motion, while the frequencies of the swaying motion are 5s, 7s, and 6s respectively. The initial phase are $\theta_0 = 0°, \gamma_0 = 0°$ and $\psi_0 = 0°$ respectively. The IMU is simulated, where the gyro bias is $0.02°/h$ and the accelerometer accuracy is 100μ g. The outputs rate of the IMU are set as 200Hz. The scale factor of DVL is set as 1.002, and outputs rate is 1Hz. The corresponding moving trajectory and state are shown in Figure 13. For 0s∼25s, the vehicle moves linearly; for 25s∼565s, the vehicle turns 270° at the angular velocity 0.5°/s; for 565s∼1235s, the vehicle enters the linear motion; for 1235s∼1535s, the vehicle turns the angle is 180°, at which the angular velocity is 0.6°/s; for 1535s∼2000s, the vehicle moves linearly.
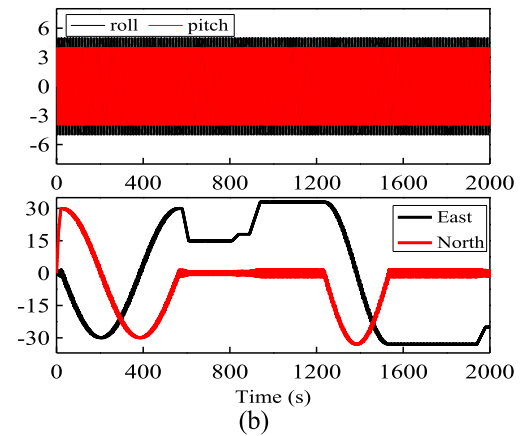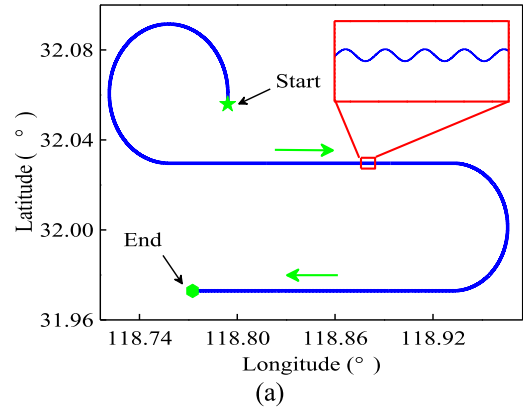
FIGURE 13. (a) Curve of moving trajectory and (b) curves of velocity and attitude.

As can be seen from Figure 13(b), the curve of the pitch angle and the roll angle is a sinusoidal curve which shows the actual underwater vehicle motion. Since the vehicle oscillates continuously throughout the process, the velocity curve appears as a local sinusoidal fluctuation, which to some extent conforms to the actual running state of the underwater vehicle.

To compare the performance of proposed Kalman filter aided by motion attitude assist (KF-MAA) method, an INS/DVL integrated navigation system based on Kalman filter (KF) is realized in this paper. The results shown in Figure 14, where the KF and KF-MAA are marked by red lines and blue lines respectively. Figure 14(a) displays the curves of the north and east velocity errors. Figure 14(b) shown the curves of the north and east position errors for KF and KF-MAA. Compared with KF, it can be seen that KF-MAA has smaller velocity error and position error.

In order to intuitively compare the effects of the two methods, the horizontal position error for the KF and KF-MAA are drawn in Figure 15, which can be seen that the position accuracy based on KF-MAA is better than the KF. In order to further compare the performance of the two methods, the above error data is analyzed, and the root mean square error (RMSE) is introduced, the results of whose results are listed in Table 3.
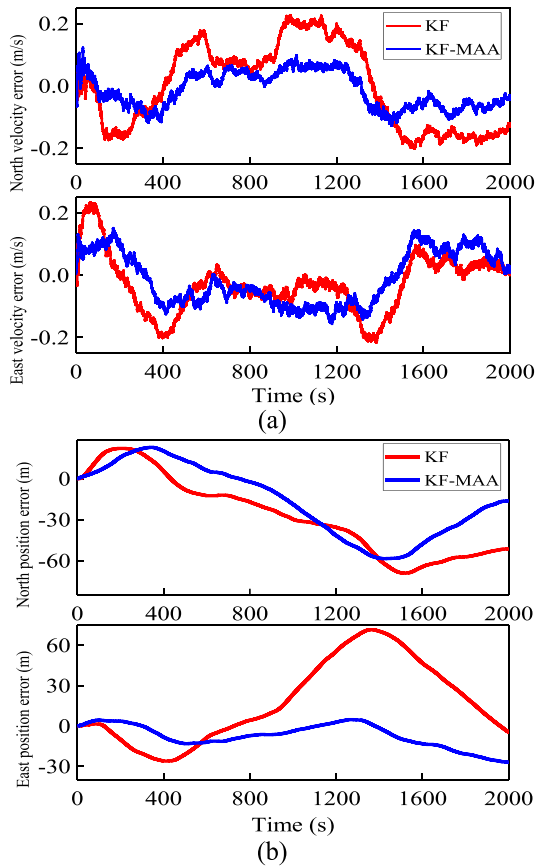
FIGURE 14. Curves of the velocity errors (a) and position errors (b) for KF and KF-MAA.
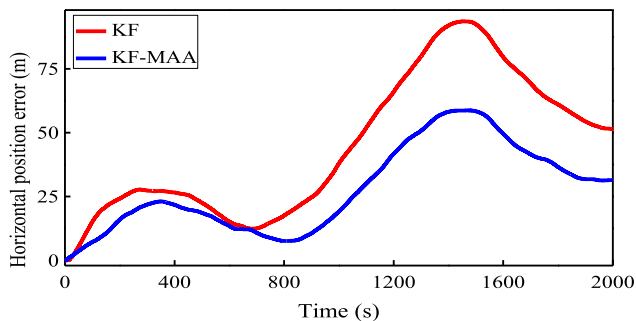

FIGURE 15. Curves of the horizontal position errors for KF and KF-MAA.

We can see that the east and north max velocity error for KF-MAA are 0.151m/s and 0.123m/s respectively, which reduced by 35.7% and 46.1% than KF method for INS/DVL integrated navigation system. From the analysis of the position error statistics, the max error and mean error of KF-MAA method are less than KF method such as east position, north position and horizontal position. Taking the horizontal position error as an example, the max error, mean error and RMSE of horizontal position for KF are 93.610m, 44.865m, and 27.341m respectively. However, the max error, mean error, and RMSE of horizontal position for KF-MAA are 58.730m, 28.106m, and 16.863m respectively, whose

TABLE 3. Velocity errors and position errors analysis for KF and KF-MAA.

	Method	Max	Mean	RMSE
East velocity error	KF	0.235	-0.030	0.090
(m/s)	KF-MAA	0.151	-0.012	0.084
North velocity	KF	0.228	-0.003	0.135
error (m/s)	KF-MAA	0.123	-0.014	0.058
East position error	KF	71.628	17.725	30.135
(m)	KF-MAA	4.718	-7.254	8.675
North position	KF	-69.083	-27.091	28.358
error (m)	KF-MAA	-58.519	-16.363	26.070
Horizontal	KF	93.610	44.865	27.341
position error (m)	KF-MAA	58.730	28.106	16.862

accuracy increased by 37.3%, 37.4%, and 38.3% respectively. Therefore, the integrated navigation method aided by MAA can reduce the velocity and position error as well as improving the accuracy effectively.

The root mean square error is the arithmetic square root of the variance that reflects the degree of dispersion of a data set. The smaller the root mean square error, the higher the accuracy of the data. From table 3 we can see that the RMSE value of east velocity and north velocity for KF-MAA are 0.084m/s and 0.058m/s respectively, which reduced by 6.7% and 57.0% than KF method.Meanwhile, the RMSE value of east position, north position and horizontal position for KF-MAA are 8.675m, 26.070m and 16.862m respectively, which reduced by 71.2%, 8.1% and 38.3% than KF method. According to the RMSE analysis, the KF-MAA method proposed in this paper has a small RMSE value compared with KF in terms of velocity error and position error. Therefore, the KF-MAA method has better performance in terms of navigation accuracy.

B. TESTING IN A VEHICULAR ENVIRONMENT

Vehicle test experiment is used to simulate underwater vehicle due to the limitations of the experimental conditions. This test systems consisted of a navigation grade INS PHINS of IXSEA Corporation, a fiber optical gyro (FOG), and a FlexPark 6 GPS receiver of NovAtel Corporation. Meanwhile, PHINS is utilized as a reference system to provide the accurate navigation information. PHINS is introduced in the test not only as an inertial navigation system, the integrated navigation system structure is shown in figure 16(c). In vehicle test, PHINS is combined with the GPS receiver. Therefore, PHINS works on INS/GPS combined navigation mode. From this point of view, PHINS provides relatively accurate speed, and due to the existence of GPS navigation information, the speed error accumulation of PHINS is small. The vehicle equipment and trajectory of the test are shown in Figure 16. PHINS that provides velocity information can pretend to be a DVL by adding noise and scale factor. We have obtained the installation error between IMU and PHINS through the calibration experiment, which is $\phi_x = 0.04^o$, $\phi_y = 0.03^o$, $\phi_z = 1.5^o$. In this experiment we have compensated for the installation error, and ignore other DVL errors. The instrument specifications are listed in Table 4.
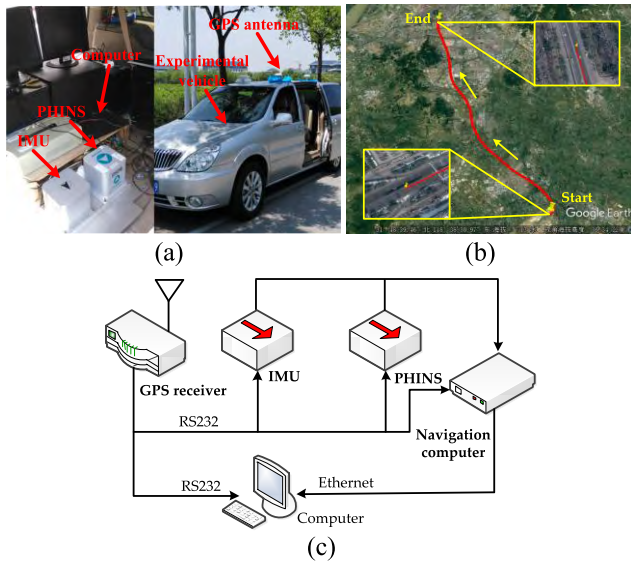
FIGURE 16. (a) Vehicle equipment, (b) the trajectory of the test, (c) Integrated navigation system structure.

TABLE 4. Instrument specifications.

Instruments	Parameters	Accuracy	Frequency
IMU	Gyroscope bias stability	$\leq 0.02^{o}/h(1\sigma)$	200Hz
	Gyroscope random walk	$\leq 0.005^{o}/\sqrt{h}$	200Hz
	Accelerometer bias variation	$\pm 50ug$	200Hz
	Accelerometer output noise	$\leq 50ug/\sqrt{Hz}$	200Hz
GPS	Velocity (RMS)	0.03m/s	1Hz
	Position (L1)	1.5m	1Hz
PHINS	Attitude (GPS aided mode)	$\leq 0.01^{o}$	200Hz

In the vehicle experiment, due to the complicated external environment, it is considered that the test data contains other colored noise. The whole test lasts for 1500s. Figure 17 shows the curves of the velocity (a) and attitude (b) in the entire vehicle test process.

First, the gyro de-noising algorithm based on the improved AR model is verified. Gyro signal is collected while the vehicle is stationary, and the parameters are identified by the proposed MRLS algorithm. Figure 18(a) and (b) show the real-time estimation results of the parameters and constant c.

As can be seen from the Figure 18, in the absence of disturbance, the estimated parameters tend to become stable in about 200s, and the estimated values are as follows:

$$\varphi_1 = -0.5984, \varphi_2 = 0.3761, \varphi_3 = 0.2449, c = 0.00000674 \quad (35)$$

Therefore, the improved AR (3) model is:

$$z_k = -0.5984z_{k-1} + 0.3761z_{k-2} + 0.2449z_{k-3} + 0.00000674 + a_k \quad (36)$$
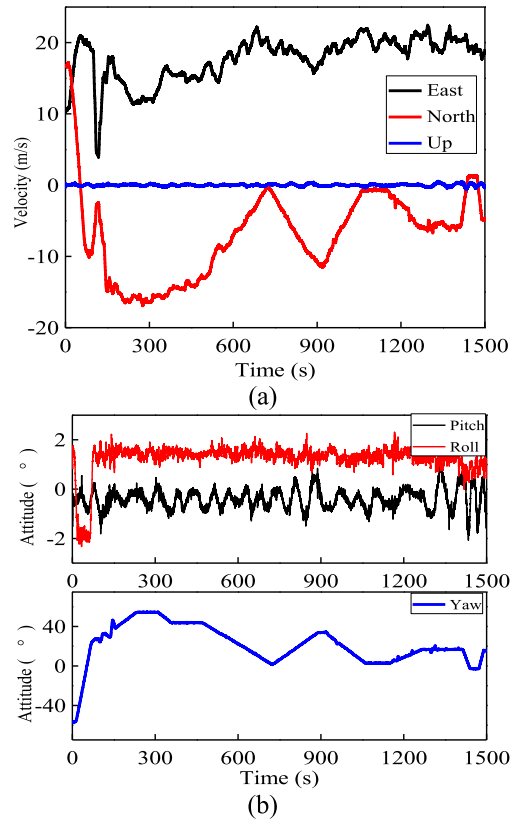

FIGURE 17. Curves of the velocity (a) and attitude (b) with vehicle test.

Then, the equation Kalman filter 1 in figure 2 is:

$$\begin{bmatrix} z_k \\ z_{k-1} \\ z_{k-2} \\ c \end{bmatrix} = \begin{bmatrix} -0.5984 & 0.3761 & 0.2449 & 1 \\ 1 & 0 & 0 & 0 \\ 0 & 1 & 0 & 0 \\ 0 & 0 & 0 & 1 \end{bmatrix} \begin{bmatrix} z_{k-1} \\ z_{k-2} \\ z_{k-3} \\ c \end{bmatrix}$$
$$+ \begin{bmatrix} 1 & 0 & 0 & 0 \\ 0 & 0 & 0 & 0 \\ 0 & 0 & 0 & 0 \\ 0 & 0 & 0 & 0 \end{bmatrix} \begin{bmatrix} a_k \\ 0 \\ 0 \\ 0 \end{bmatrix} \quad (37)$$

$$z_k = \begin{bmatrix} 1 & 0 & 0 & 0 \end{bmatrix} \begin{bmatrix} z_k & z_{k-1} & z_{k-2} & c \end{bmatrix}^T + v_k \quad (38)$$

According to the above process model and observation model, the gyro signal is subjected to real-time de-nosing by the Kalman filter 1, and the INS/DVL integrated navigation system is performed. Figure 19(a) and (b) display velocity errors and horizontal position errors for two methods.

It can be seen from Figure 19 that the velocity errors and position errors of the integrated navigation are significantly reduced after de-noising. Figure 19(a) shows that the mean square error (MSE) of the east velocity error after noise reduction and no noise reduction are 0.01632 and, 0.01859 respectively. The de-noising method based on AR model effectively reduces the gyro noise and improves the INS/DVL integrated navigation accuracy. Since the underwater carrier has long voyage characteristics, the method works better in long-time integrated navigation.
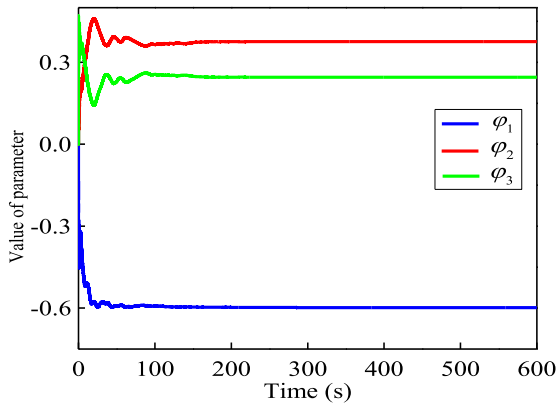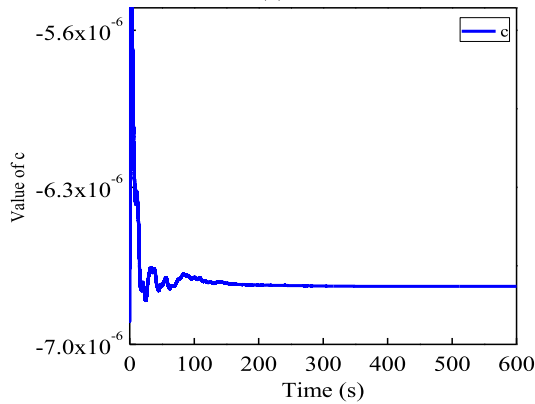
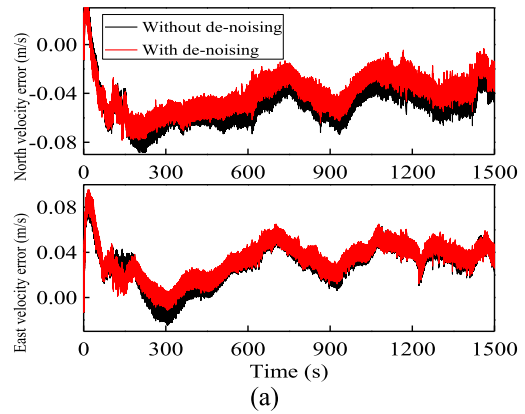**FIGURE 18.** Real-time estimation of the parameters (a) and constant c (b).

FIGURE 19. Curves of the velocity errors (a) and horizontal position errors (b) for two methods.

Based on the de-noising method, the KF and KF-MAA are introduced in INS/DVL integrated navigation system to evaluate the performance of KF-MAA method. Figure 20(a) and (b) display the curves of the velocity errors and position errors for KF and KF-MAA. Figure 21 shows the curve of the horizontal position errors for different methods.
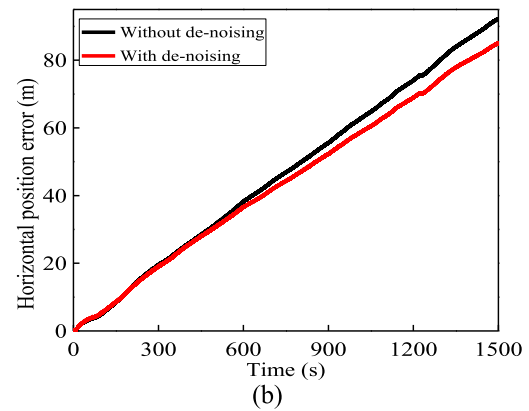
As can be seen in Figure 20 and 21, the velocity and position errors of the integrated navigation are reduced after aided by MAA, so the KF-MAA enhances the accuracy of DVL velocity. The Figure 21 shows that the position error based on KF is rapid divergence with time, but the position error of INS/DVL system based on KF-MAA is slow. It can be seen that proposed method is superior in the case of long-haul time. Based on the above analysis, the statistical analysis of the position errors for different methods are listed in Table 5.

On the one hand, Table 5 shows that in the 1500s vehicle test, the max horizontal position error of the integrated navigation with de-noising and without de-noising are 85.049m and 92.241m respectively. The position accuracy is improved by 7.79%. On the other hand, the max horizontal position error of the proposed approach is 77.460m, which is 16.02% higher than the traditional KF-based method.

To further evaluate the performance of the proposed approach, the DVL outage areas are added to the vehicle test. The trajectory of the test with DVL outages is shown in Figure 22, where three DVL outages (60s, 90s, and 120s) are marked by red lines such as #1 (350s~410s), #2 (750s~840s), and #3 (1200s~1310s).

Figure 23(a) and (b) show the curves of velocity errors with DVL outages such as north, east and horizontal velocity. We know that the proposed approach has the smallest horizontal velocity error than other methods in DVL outage areas.

The velocity errors analysis results are listed in Table 6. It can be seen from Table 6 that in the three time periods #1, #2, and #3 of the DVL outage, the max horizontal velocity errors of the integrated navigation with de-noising are 0.061 m/s, 0.098 m/s, and 0.03 m/s respectively. Comparing to the results of without de-nosing, the accuracy are increased by 10.29%, 14.78%, and 16.66% respectively. Meanwhile, the max horizontal velocity errors of the proposed
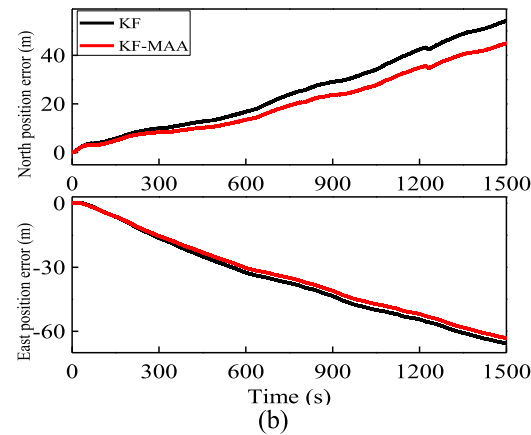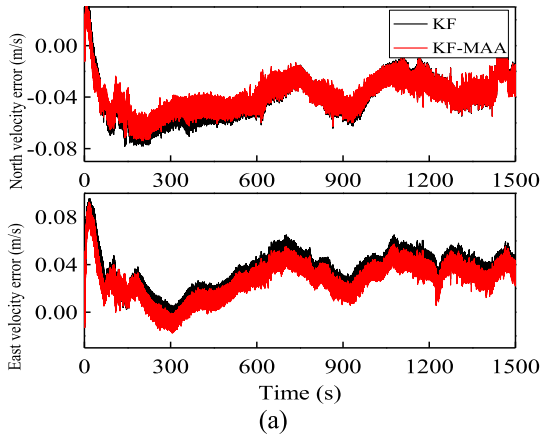
TABLE 5. Position errors for different methods.

	Without de-noising (m)		With de-noising (m)		Proposed approach (m)	
	Max	Mean	Max	Mean	Max	Mean
East	-77.76	-40.63	-65.6	-35.52	-63.13	-33.93
North	49.62	22.43	50.13	23.02	44.89	20.93
Horizontal	92.24	46.58	85.04	43.85	77.46	39.76

FIGURE 20. Curves of the velocity errors (a) and position errors (b) for KF and KF-MAA.
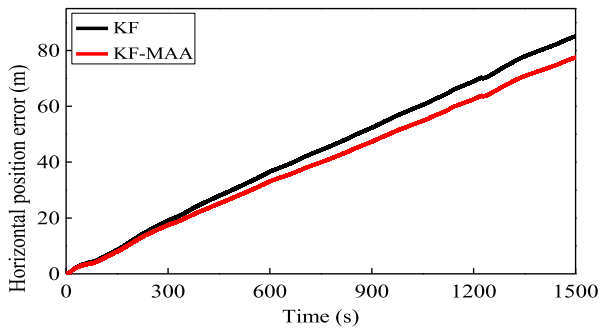
FIGURE 21. Curve of the horizontal position errors for KF and KF-MAA.

FIGURE 22. The trajectory of the test with DVL outages.

FIGURE 23. (a) Curves of the north and east velocity errors with DVL outages and (b) curve of horizontal velocity errors with DVL outages.

approach are 0.063m/s, 0.086m/s and 0.024m/s respectively, which are 7.35%, 25.22% and 33.33% higher than KF method.

Figure 24(a) and (b) show the curves of the north, east and horizontal position errors with DVL outages. The max horizontal position error of without de-noising and with de-noising are 78.799m and 74.168m respectively. Its positional accuracy is improved by 5.87%. Meanwhile, the max horizontal position error of the proposed approach is 69.192m, which is 12.19% higher than the traditional KF method.
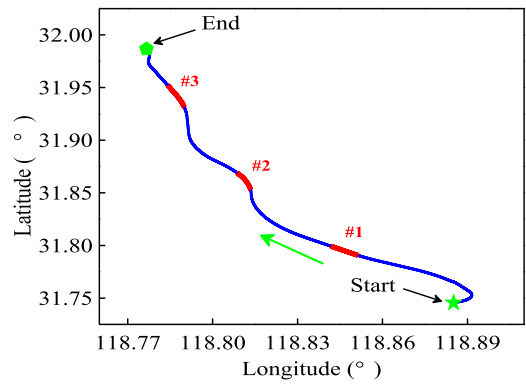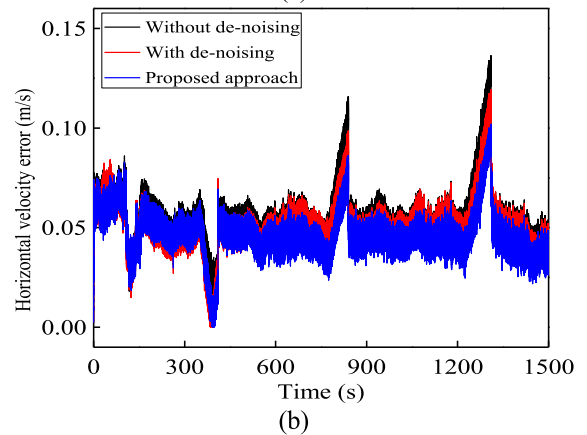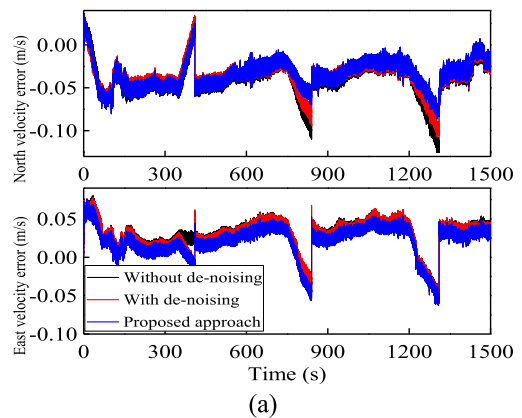
The above results show that the proposed approach can still maintain high navigation accuracy compared with the traditional KF method in the case of DVL outage. On the one hand, the real-time de-noising method proposed in this paper can suppress the error of the INS when the DVL outage. On the other hand, the real-time de-noising method based on the improved AR model and the MAA simultaneously improves the accuracy of the INS/DVL integrated navigation system when the DVL data is valid.

TABLE 6. Velocity errors analysis results with DVL outages.

|		Without de-noising		With de-noising		Proposed approach	
		Max	Mean	Max	Mean	Max	Mean
#1	East (m/s)	0.015	0.025	-0.017	0.007	-0.017	0.003
	North (m/s)	0.024	-0.019	0.033	-0.010	0.025	-0.017
	Horizontal (m/s)	0.068	0.036	0.061	0.023	0.063	0.023
#2	East (m/s)	-0.045	-0.001	-0.040	0.001	-0.056	-0.009
	North (m/s)	-0.109	-0.062	-0.093	-0.054	-0.069	-0.041
	Horizontal (m/s)	0.115	0.068	0.098	0.060	0.086	0.049
#3	East (m/s)	-0.059	-0.011	-0.086	-0.012	-0.062	-0.016
	North (m/s)	-0.125	-0.073	-0.107	-0.062	-0.086	-0.050
	Horizontal (m/s)	0.036	0.078	0.030	0.068	0.024	0.058
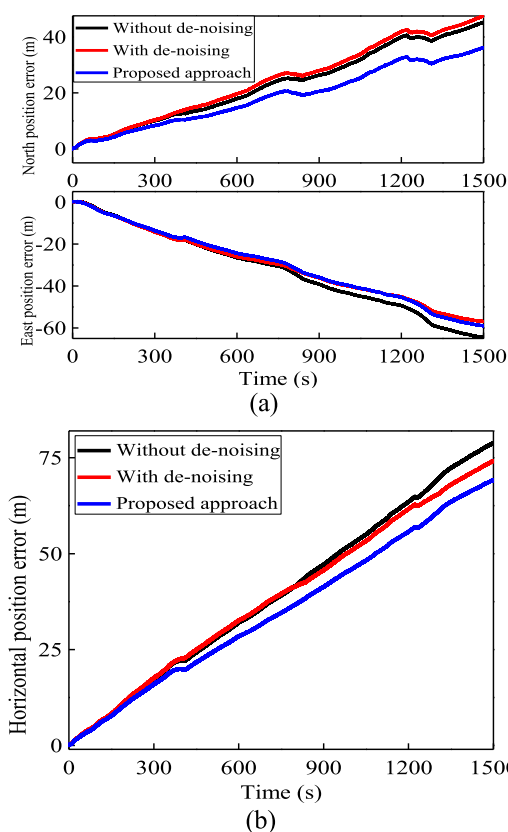
FIGURE 24. (a) Curves of the north and east position errors with DVL outages and (b) curve of horizontal position errors with DVL outages.

VI. CONCLUSIONS

KF has been widely used as a common method in the INS/DVL integrated navigation system. Based on this, a hybrid approach is proposed in this paper. On the one hand, a real-time de-noising method is introduced for gyro signal. On the other hand, a error compensation method is proposed to compensate DVL velocity errors due to swing of the vehicle. The simulations and vehicle experiments show that the proposed approach has higher navigation accuracy than the KF method, and the following three contributions are obtained:

1. The DVL error compensation method based on MAA is proposed under complex motion conditions.
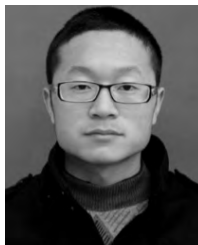
2. An modified RLS algorithm is designed for AR model parameters.

3. The real-time de-noising method based on the improved AR model is introduced to improve the INS navigation accuracy, especially under long-term working conditions.

REFERENCES

[1] L. Paull, S. Saeedi, M. Seto, and H. Li, "AUV navigation and localization: A review," *IEEE J. Ocean. Eng.*, vol. 39, no. 1, pp. 131–149, Jan. 2014.

[2] B. Allotta *et al.*, "Typhoon at CommsNet13: Experimental experience on AUV navigation and localization," *Annu. Rev. Control*, vol. 40, no. 10, pp. 157–171, 2015.

[3] X. Xu, X. Xu, Y. Yao, and Z. Wang, "In-motion coarse alignment method based on reconstructed observation vectors," *Rev. Sci. Instrum.*, vol. 88, no. 3, 2017, Art. no. 035001.

[4] Da-X. Ji, W. Song, H.-Y. Zhao, and J. Liu, "Deep sea AUV navigation using multiple acoustic beacons," *China Ocean Eng.*, vol. 30, no. 2, pp. 309–318, 2016.

[5] M. T. Sabet, H. M. Daniali, A. Fathi, and E. Alizadeh, "A low-cost dead reckoning navigation system for an AUV using a robust AHRS: Design and experimental analysis," *IEEE J. Ocean. Eng.*, vol. 43, no. 4, pp. 927–939, Oct. 2018.

[6] Ø. Hegrenaes and O. Hallingstad, "Model-aided INS with sea current estimation for robust underwater navigation," *IEEE J. Ocean. Eng.*, vol. 36, no. 2, pp. 316–337, Apr. 2011.

[7] M. Karimi, M. Bozorg, and A. R. Khayatian, "A comparison of DVL/INS fusion by UKF and EKF to localize an autonomous underwater vehicle," in *Proc. 1st RSI/ISM Int. Conf. Robot. Mechatron. (ICRoM)*, Feb. 2013, pp. 62–67.

[8] M. Dinc and C. Hajiyev "Integration of navigation systems for autonomous underwater vehicles," *J. Mar. Eng. Technol.*, vol. 14, no. 1, pp. 32–43, 2015.

[9] I. Klein and R. Diamant, "Observability analysis of DVL/PS aided INS for a maneuvering AUV," *Sensors*, vol. 15, no. 10, pp. 26818–26837, 2015.

[10] N. Davari and A. Gholami, "An asynchronous adaptive direct Kalman filter algorithm to improve underwater navigation system performance," *IEEE Sensors J.*, vol. 17, no. 4, pp. 1061–1068, Feb. 2017.

[11] M. Emami and M. R. Taban, "A low complexity integrated navigation system for underwater vehicles," *J. Navigat.*, vol. 71, no. 5, pp. 1161–1177, 2018.

[12] X. Liu, X. Xu, Y. Liu, and L. Wang, "Kalman filter for cross-noise in the integration of SINS and DVL," *Math. Problems Eng.*, vol. 2014, Mar. 2014, Art. no. 260209.

[13] Y. Yao, X. Xu, and X. Xu, "An IMM-aided ZUPT methodology for an INS/DVL integrated navigation system," *Sensors*, vol. 17, no. 9, p. 2030, 2017.

[14] Y. Guo, M. Wu, K. Tang, and L. Zhang, "Square-root unscented information filter and its application in SINS/DVL integrated navigation," *Sensors*, vol. 18, no. 7, p. 2069, 2018.

[15] A. Tal, I. Klein, and R. Katz, "Inertial navigation system/Doppler velocity log (INS/DVL) fusion with partial DVL measurements," *Sensors*, vol. 17, no. 2, p. 415, 2017.

[16] L. Yi-Ting, X. Xiao-Su, L. Xi-Xiang, Z. Tao, L. Yao, Y. Yi-Qing, W. Liang, and T. Jin-Wu, "A fast gradual fault detection method for underwater integrated navigation systems," *J. Navigat.*, vol. 69, no. 1, pp. 93–112, 2016.

[17] X. Xu, P. Li, and J.-J. Liu, "A fault-tolerant filtering algorithm for SINS/DVL/MCP integrated navigation system," *Math. Problems Eng.*, vol. 2015, Apr. 2015, Art. no. 581909.

[18] Y. Kang, L. Zhao, J. Cheng, M. Wu, and X. Fan, "A novel grid SINS/DVL integrated navigation algorithm for marine application," *Sensors*, vol. 18, no. 2, p. 364, Jan. 2018.

[19] Y. Zhu, X. Cheng, J. Hu, L. Zhou, and J. Fu, "A novel hybrid approach to deal with DVL malfunctions for underwater integrated navigation systems," *Appl. Sci.*, vol. 7, no. 8, p. 759, 2017.

[20] P. Liu, B. Wang, Z. Deng, and M. Fu, "INS/DVL/PS tightly coupled underwater navigation method with limited DVL measurements," *IEEE Sensors J.*, vol. 18, no. 7, pp. 2994–3002, Apr. 2018.

[21] J. Sun, X. Xu, Y. Liu, T. Zhang, and Y. Li, "FOG random drift signal denoising based on the improved AR model and modified Sage-Husa adaptive Kalman filter," *Sensors*, vol. 16, no. 7, p. 1073, 2016.

[22] L. Huang, Z. Li, F. Xie, and K. Feng, "Novel time series modeling methods for gyro random noise used in Internet of Things," *IEEE Access*, vol. 6, pp. 47911–47921, 2018.

[23] J. Q. Bai, K. Zhang, and Y. X. Wei, "Modeling and analysis of fiber optic gyroscope random drifts," *J. Chin. Inert. Technol*, vol. 20, no. 5, pp. 621–624, 2012.

[24] L. Huang, "Auto regressive moving average (ARMA) modeling method for Gyro random noise using a robust Kalman filter," *Sensors*, vol. 15, no. 10, pp. 25277–25286, 2015.

[25] T. S. Choe, W. S. Ra, and J. B. Park, "Depth sensor and DVL-aided vertical channel damping loop design for underwater vehicles," *Electron. Lett.*, vol. 51, no. 22, pp. 1763–1765, 2015.

[26] P. Liu, B. Wang, Z. Deng, and M. Fu, "A correction method for DVL measurement errors by attitude dynamics," *IEEE Sensors J.*, vol. 17, no. 14, pp. 4628–4638, Jul. 2017.

[27] Z. Yonggang, D. Yan, and L. Ning, "A tightly integrated SINS/DVL navigation method for autonomous underwater vehicle," in *Proc. Int. Conf. Comput. Inf. Sci. (ICCIS)*, Jun. 2013, pp. 1107–1110.

[28] A. A. Nakhaei, M. S. Helfroush, H. Danyali, and M. Ghanbari, "Subjectively correlated estimation of noise due to blurriness distortion based on auto-regressive model using the Yule–Walker equations," *IET Image Process.*, vol. 12, no. 10, pp. 1788–1796, 2018.

XIAOSU XU received the Ph.D. degree from the School of Automation, Southeast University, Nanjing, China, in 1991. He is currently a Professor with the School of Instrument Science and Engineering, Southeast University, and the Director of the Key Laboratory of Micro Inertial Instrument and Advanced Navigation Technology, Ministry of Education, China. His current research interests include inertial navigation and combination navigation techniques.

YIQING YAO received the Ph.D. degree from the School of Instrument Science and Engineering, Southeast University, Nanjing, China, in 2018. She is currently a Lecturer with the School of Instrument Science and Engineering, Southeast University, and the Key Laboratory of Micro Inertial Instrument and Advanced Navigation Technology, Ministry of Education, China. Her current research interests include inertial navigation and integrated navigation systems.

YONGYUN ZHU was born in Xinxiang, Henan, in 1991. He is currently pursuing the Ph.D. degree in instrument science and technology with Southeast University, Nanjing, China. His research interests include initial alignment for inertial navigation, integrated navigation for autonomous underwater vehicles, ship's acoustic navigation systems, USBL, and information fusion.

DI WANG received the B.S. degree in electronic science and technology from Jiangsu Normal University, Xuzhou, Jiangsu, in 2015, and the M.S. degree in control science and engineering from Lanzhou Jiaotong University, Lanzhou, Gansu, China, in 2018. He is currently pursuing the Ph.D. degree in navigation, guidance, and control with Southeast University, Nanjing. His research interests include inertial navigation and integrated navigation technology, INS/GPS integrated algorithms, and INS/DVL integrated algorithms, which is applied in the field of underwater navigation technology.

JINWU TONG was born in Wuhan, Hubei, China. He was from Liuyang, Hunan, China. He received the B.S. degree in computer science and technology from Central South University, Changsha, Hunan, in 2007, and the M.S. degree in control science and engineering from the Guilin University of Electronic Technology, Guilin, China, in 2013. He is currently pursuing the Ph.D. degree in instrument science and technology with Southeast University, Nanjing, Jiangsu.

His research interests include inertial device test and calibration, the initial alignment of strap down inertial navigation systems (SINS), underwater navigation and positioning, underwater acoustic navigation device tests and error calibration, SINS/GNSS, SINS/LBL, SINS/SBL, SINS/USBL integrated navigation, medical image processing, machine learning, and artificial intelligence pathology diagnosis.

• • •